





ARTICLE OPEN



Degradation of Cu nanowires in a low-reactive plasma environment

Diego S. R. Coradini^{1,4}, Matheus A. Tunes^{1,4}, Thomas M. Kremmer¹, Claudio G. Schön², Peter J. Uggowitzer^{1,3} and Stefan Pogatscher¹

The quest for miniaturisation of electronic devices is one of the backbones of industry 4.0 and nanomaterials are an envisaged solution capable of addressing these complex technological challenges. When subjected to synthesis and processing, nanomaterials must be able to hold pristine its initial designed properties, but occasionally, this may trigger degradation mechanisms that can impair their application by either destroying their initial morphology or deteriorating of mechanical and electrical properties. Degradation of nanomaterials under processing conditions using plasmas, ion implantation and high temperatures is up to date largely sub-notified in the literature. The degradation of single-crystal Cu nanowires when exposed to a plasma environment with residual active O is herein investigated and reported. It is shown that single-crystal Cu nanowires may degrade even in low-reactive plasma conditions by means of a vapour–solid–solid nucleation and growth mechanism.

npj Materials Degradation (2020)4:33; <https://doi.org/10.1038/s41529-020-00137-2>

INTRODUCTION

The advent of nanoscaled materials such as nanoparticles (NPs), nanotubes (NTs) and nanowires (NWs) has been subjected to intense research studies in the recent years given their reported electrical, mechanical and optical properties which differ from bulk materials mainly due to the large surface-to-volume ratio (SVR)^{1,2}. This set of properties explains the wide range of suggested applications that nanomaterials face nowadays in several areas of industry and science such as biomedical and electronics industries^{3–6}.

A recent application of nanomaterials involves miniaturisation of electronic circuits and devices which has potential to revolutionise the electronics industry^{7–12}, not only by extending the validity of Moore's law, but exceeding the scientific vision beyond it^{13–15}. In this context, the search for reliable synthesis and processing routes for nanomaterials remains a significant challenge for academia and technology companies: for example, the ion-beam-induced processing doping of semiconductor nanowires was shown to severely degrade them via mechanisms known as ion-induced bending^{16,17}. Additional studies exploring degradation effects (from distinct and/or multiple sources operating synergistically) in nanomaterials are still largely required.

Despite the ongoing research and industrial interest on the semiconductor branch, metallic nanomaterials are also focusing the attention of the scientific community due to the recently reported superior properties when compared with their metallic bulk form¹⁸. Among the wide variety of metallic nanomaterials under investigation, Cu is commonly used in the microelectronics industry due to its suitable cost–benefit and appropriate mechanical and electrical properties¹⁹. As an example, in its oxide form, it has been discovered that Cu can be used as a one-dimensional nanostructure with envisaged applications in solar cells, gas and humidity sensors, high-temperature conductors and field emitter miniaturised transistors^{3,20,21}. Many of these

applications are related with its narrow band gap that varies from 1.2 to 2.1 eV (both CuO and Cu₂O are p-type semiconductors) at room temperature^{3,20,21}.

Nevertheless, the applicability of metallic nanomaterials like Cu NWs in nanocircuitry may be impaired when the thermodynamic stability of its (metallurgical) phase upon exposure to degradation environments is considered². The use of Cu can be limited by its susceptibility to oxidation at low temperatures²², resulting in the formation of a partial self-passivation layer as opposed to Al which reacts with O creating a more uniform and continuous self-passivation layer^{19,22,23}. In addition, as observed in thin films, the reaction with monoatomic O and/or O₂-rich environments may induce the formation of oxides like CuO and Cu₂O which can degrade the initial electrical and mechanical properties of pure Cu²².

An important requirement of microelectronics is the appropriate cleaning of materials and devices before and after their processing. The presence of carbonaceous impurities may destroy the component or reduce its initial designed functionality. A method frequently used by industry to carry out such cleaning is via the use of plasma which can remove superficial impurities by means of physical processes such as ablation, bombardment, physio- and/or chemisorption^{19,24–26}. Besides cleaning the surface of a material, plasma has been also used in inorganic nanostructure fabrication^{27–29}. The latter fact is due to the distinct physicochemical properties of plasma such as the presence of several ionised chemical species that have a high reactivity with some metallic surfaces^{3,6,29–32}. For application in electron microscopy, for example, plasma cleaning devices are designed to neither induce heat nor sputtering of samples, but to remove the outermost layers of surface contamination (in a form of carbonaceous impurities and/or C–H-based weakly bonded contaminants)³³. Notwithstanding, the presence of active species in a plasma environment can also lead to undesired degradation effects in nanomaterials, but to the best of our knowledge, there is

¹Chair of Non-Ferrous Metallurgy, Montanuniversitaet Leoben, Leoben, Austria. ²Department of Metallurgical and Materials Engineering, Escola Politécnica da Universidade de São Paulo, São Paulo, Brazil. ³Laboratory of Metal Physics and Technology, Department of Materials, ETH Zürich, Zürich, Switzerland. ⁴These authors contributed equally: Diego S. R. Coradini, Matheus A. Tunes. ✉email: diego.sr.coradini@unileoben.ac.at; m.a.tunes@physics.org

a current lack of reports regarding the effects of reactive plasma exposure in Cu NWs.

Although the low- or high-reactive plasma degradation of NWs is largely sub-notified in the literature, several authors reported degradation effects of plasma on metallic thin films. Gibson et al.⁷ observed the effects of a simulated plasma environment (similarly to that found in low earth orbit) on a Cu thin films by analysing interaction of monoatomic O with their surfaces. In the study, the authors observed that the Cu thin films (Cu_2O) had a higher reactivity with monoatomic O than with molecular O (i.e. O_2), even in low-pressure conditions (0.0013 mbar)⁷. This was similarly investigated by Kennedy and Friesen⁹ whose concluded that the growth of Cu films via sputtering processes can be affected by the O partial pressure and that the presence of a low-content O atmosphere can lead to adsorption, which upon segregation at the surface may initiate oxide layer growth.

The effects of plasma exposure in nanomaterials has been recently reviewed by Ostrikov et al.³⁰ who also were pioneers to investigate the degradation effects of a high-reactive (O-rich) plasma environment on metallic substrates in promoting nucleation and growth of different types of metal oxide NWs. In this context, two distinct physicochemical mechanisms were identified: the solid–liquid–solid (SLS) and vapour–solid–solid (VSS)³⁰ mechanisms. SLS mechanism is observed for metallic substrates with low melting point and it consists on the melting of a nanoregion caused by the reaction of the metal with the monatomic O present in the plasma. VSS mechanism is observed for metals with higher melting point, such as Fe for example. The melting of a nanoregion may also occur in the VSS, but the direct adsorption of a gas-phase into the molten-metal nanoregion (or activated nanoregion) and the higher temperatures involved with these processes can catalyse recrystallisation and growth of an oxide solid phase at the liquid–solid interface³⁰.

In the present study, the effects of low-reactive plasma exposure on Cu NWs will be reported. The NWs were characterised within a scanning/transmission electron microscope (S/TEM) before and after the plasma exposure. The low-reactive plasma is mainly composed of Ar ions with residual gases—such as O which was not intentionally added—and the initial objective was to clean the Cu NWs before electron microscopy. However, the exposure to such plasma environment revealed an unexpected degradation of the Cu NWs, which was the main motivation for

the investigations that will be reported in this study. The characterisation of this degradation effect was carried out by the detailed use of electron-microscopy techniques such as high-angle annular dark field (HAADF), energy-dispersive X-ray (EDX) spectroscopy mapping and also via conventional TEM techniques such as selected-area electron diffraction (SAED).

RESULTS

Morphology of the pristine Cu NWs

The pre-plasma exposure electron-microscopy characterisation of the Cu NWs is shown in Fig. 1. This Cu NWs condition is herein referred as pristine. SAED pattern and bright-field TEM (BFTEM) analysis, shown in Fig. 1b, c, respectively, revealed that the Cu NWs are initially single-crystalline and nanoroughness (known as “hillocks” in the literature³⁰) is noticeable on the surface of the Cu NWs. The superficial inhomogeneities observed on the Cu NWs in BFTEM were also previously reported as partial passivation layer^{23,24}. Insets in Fig. 1d–f show micrographs from the STEM analysis including HAADF, Cu and O EDX mapping measurements, respectively.

Morphology of Cu NWs after exposure to a low-reactive plasma

Typical morphologies of the Cu NWs after exposure to the low-reactive plasma environment as a function of time are shown in Fig. 2. The set of STEM micrographs, EDX maps and the SAED pattern presented in Fig. 2a shows the electron-microscopy characterisation of a typical Cu NW after 10 min of plasma exposure while the set of micrographs in Fig. 2b shows two Cu NWs after 25 min of exposure.

From the analysis presented in Fig. 2, two major experimental observations can be pointed out so far: (i) the Cu NWs—initially single-crystals—have altered their crystal structure as per exposure to the low-reactive plasma and (ii) the modification of their crystal structure is followed by the formation of small rounded-shape nuclei as can be observed in detail with brighter contrast in the HAADF micrographs. These nuclei will be hereafter referred to either nanoclusters (NCs) or nuclei. It is important to emphasise that such low-reactive plasma effect was not observed to occur on the different metallic substrates (TEM lamellae) used in this work; therefore, this phenomenon was restricted to the Cu NWs.

Analysis of pristine and plasma-exposed Cu NWs

With the EDX analysis, an elemental quantification of both Cu and O as a function of the low-reactive plasma exposure time was carried out. Figure 3 shows a plot where the atomic concentration of O was observed to increase with the plasma exposure time and a trend towards the expected composition of Cu_2O was detected. The pristine Cu NW has a passivation layer circumvolving its core as shown in the overlapped O and Cu maps in Fig. 3. By measuring the radius difference between O and the Cu in the pristine condition, the value was estimated to be 14.1 ± 1.3 nm. The overlapped O and Cu maps for the 10 and 25 min plasma-exposed Cu NWs also show the association of O both with the formed NCs and the degraded NW core.

Formation of rounded-shape NCs

The formation of rounded-shape NCs from the Cu NWs can be better assessed when looking at the surface of the metallic substrates after the plasma exposure. Figure 4a shows a Cu NWs above a pure Al substrate after 10 min of low-reactive plasma exposure. NCs are observed both at the surfaces of the NWs and as-deposited on the pure Al substrate. The latter case occurs when the nuclei are formed at the surface of the Cu NWs and then deposits onto the substrate during plasma exposure. Figure 4b shows an NCs size distribution estimated using the Cu EDX map

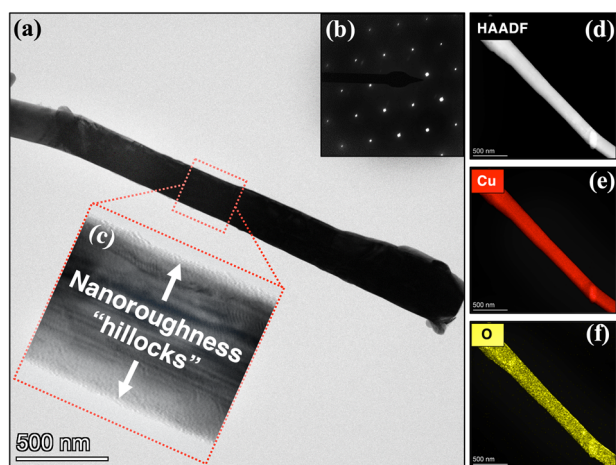


Fig. 1 Pre-plasma exposure electron-microscopy characterisation of a Cu NWs. **a** BFTEM micrograph of a Cu NW along a zone axis including **b** the SAED pattern confirming the single-crystallinity of the NWs. The BFTEM micrograph in **c** shows inhomogeneities often observed in the surface of the Cu NWs. The STEM analysis in **d–f** show the Cu NWs viewed with the HAADF detector and the Cu and O elemental maps, respectively.

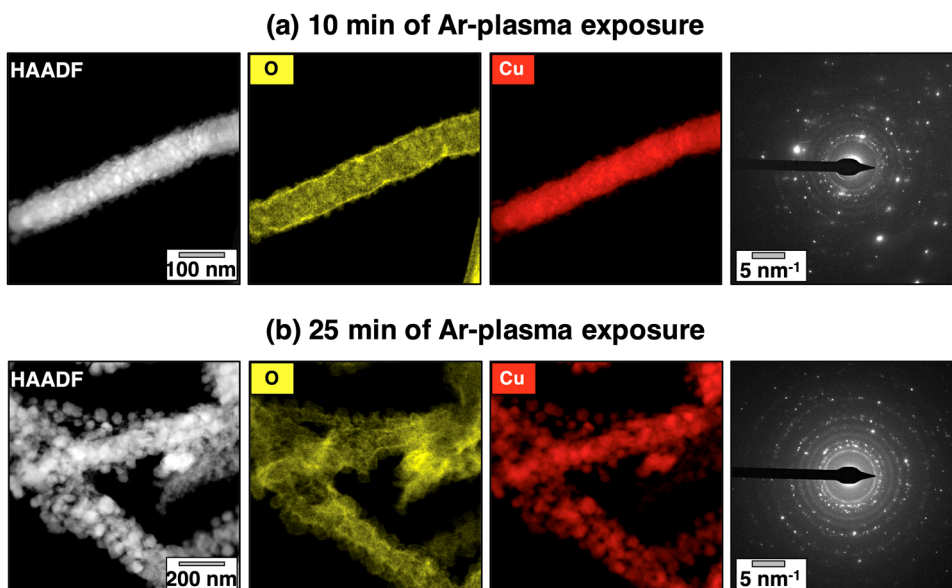


Fig. 2 Analytical electron-microscopy characterisation of the Cu NWs. After **a** 10 and **b** 25 min of low-reactive plasma exposure with their respective SAED patterns. Upon exposure to a low-reactive plasma, the initial single-crystal Cu NWs are observed to degrade to randomly oriented NCs as indicated by the SAED polycrystalline patterns in **a** and **b**.

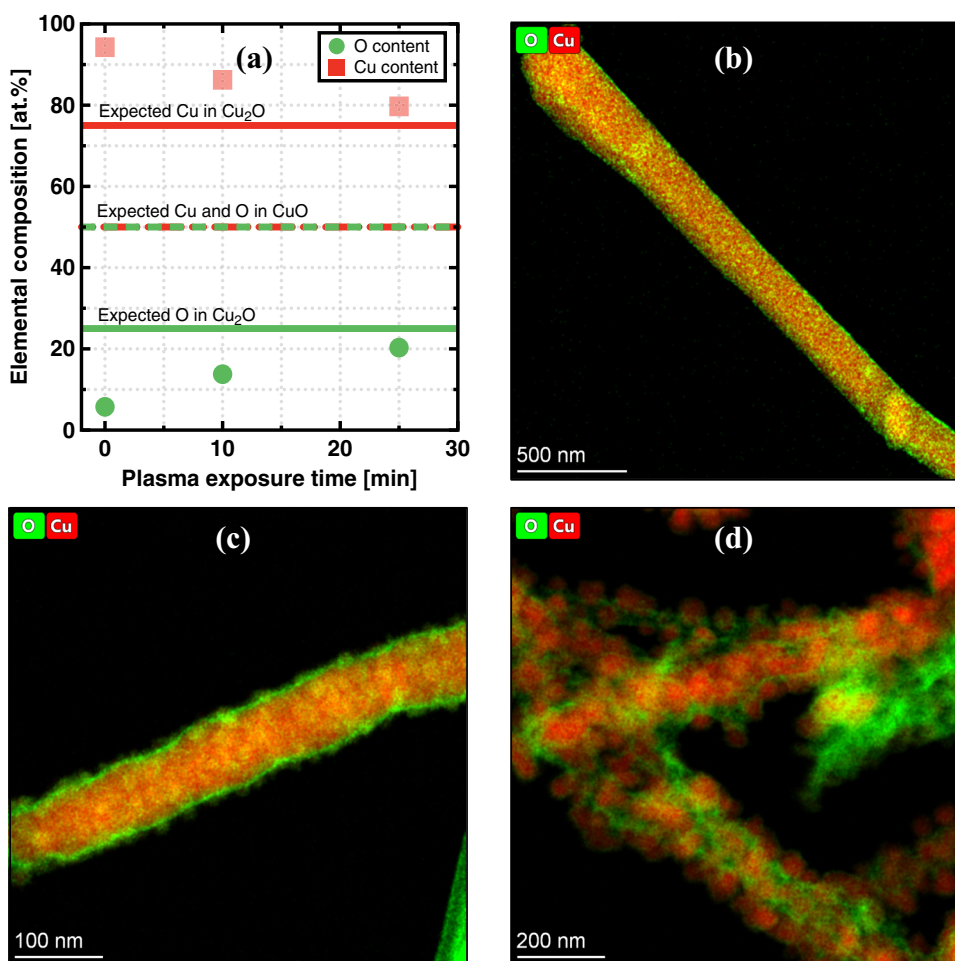


Fig. 3 Analytical characterisation of the Cu NWs plasma exposure degradation. The elemental composition of the Cu NWs before and after exposure to the low-reactive plasma is shown in plot **a**. The overlapped O and Cu elemental maps are shown for **b** pristine, **c** 10 and **d** 25 min plasma-exposed Cu NWs. As the O content was observed to increase as a function of the plasma exposure time, a trend towards the expected Cu_2O composition was noted.

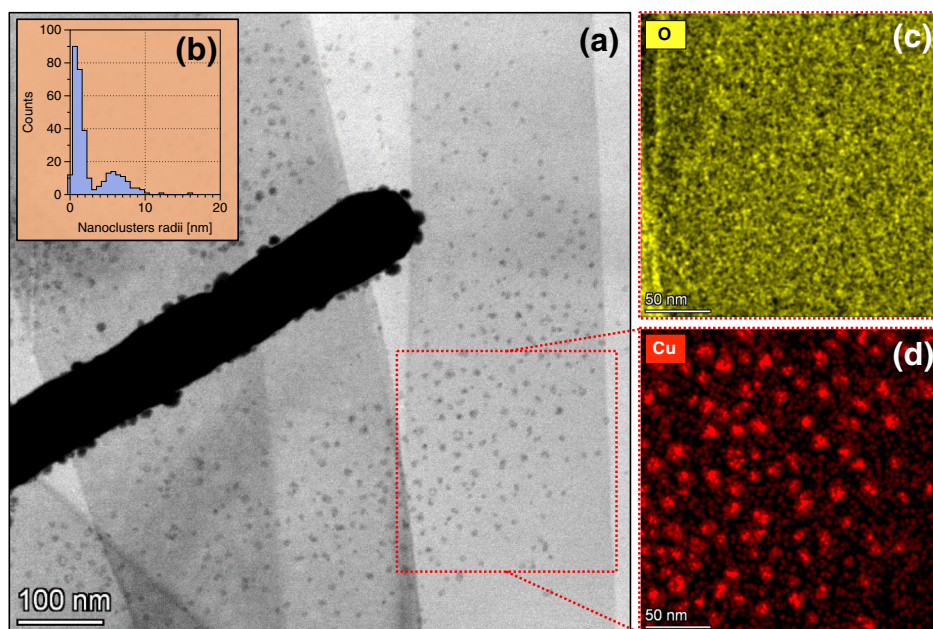


Fig. 4 Formation of rounded-shape nanoclusters. Electron-microscopy characterisation of the Cu-rich nanoclusters formed after 10 min of low-reactive plasma exposure: **a** BFTEM micrograph a Cu NWs above the pure Al substrate where some NCs are observed deposited onto it, and **b** NCs size distribution from the NCs present in the red dashed-square area. The EDX maps of O and Cu are shown in **c** and **d**, respectively, and they correspond to the red dashed-square area in **a**.

presented in Fig. 4d: the histogram of NCs radii resembles a bi-modal distribution.

The O map from the area shown as a red dashed-square in Fig. 4a revealed no significant enrichment of this element around the formed NCs. The absence of O-enrichment is also noticeable in the EDX maps presented in Fig. 2a, b.

SAED pattern indexing

SAED pattern indexing was carried out with the electron-diffraction pattern recorded from a Cu NWs after 25 min of low-reactive plasma exposure as shown in the plot in Fig. 5. This SAED pattern resembles to a polycrystalline material which is consistent with the formation of NCs. Crystallographic reference data from both Cu and Cu oxide phases (CuO and Cu₂O only) were used^{34–36}. The indexing was performed by measuring the radii of the Debye–Scherrer rings with respect to the transmitted beam. In order to improve the accuracy in measuring the rings radii (with an estimated error of 5%), the customised ImageJ script “radial profile extended” was used and the detected diffraction peaks were overlapped with the SAED pattern in Fig. 5.

These measured radii correspond to the reciprocal interplanar spacing of the potential phases present in the material system after plasma exposure. Table 1 shows experimental and crystallographic database reference values. In some cases, an overlapping between the experimental and reference interplanar spacing data from multiple phases was noticeable. By this, the following criterium was used to perform the SAED pattern indexing: (i) numerical value matching; prioritisation of planes with (ii) lower indexes and (iii) higher diffraction intensities. Using this criterium, both Cu and Cu₂O phase were indexed with higher probability of occurrence than the CuO phase.

DISCUSSION

Comparing the STEM micrographs in Figs 1d and 2a, b, it is possible to conclude that a significant morphological change of the Cu NWs has occurred as a result of low-reactive plasma exposure. Such changes are that the initial single-crystal Cu NWs

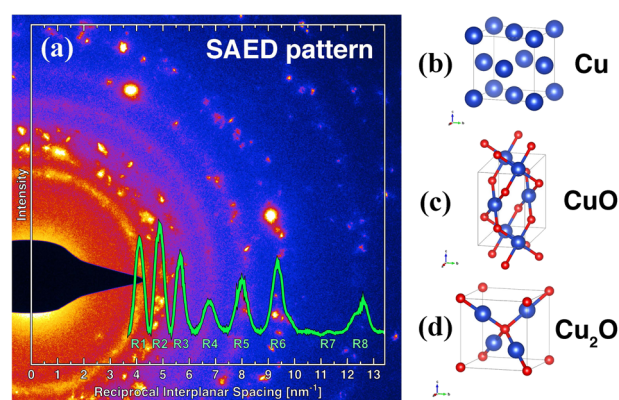


Fig. 5 Crystallographic identification of possible Cu oxide phases. **a** SAED pattern indexing using a typical electron-diffraction pattern from a Cu NW after 25 min of low-reactive plasma exposure. The diffraction peaks overlapping the SAED pattern were obtained with radial profile extended analysis within the ImageJ software. The crystallographic models for **b** Cu, **c** CuO and **d** Cu₂O were generated based on crystallographic database data available in the literature^{34–36}.

became polycrystalline upon plasma exposure and this degradation effect manifests as a function of the low-reactive plasma exposure time: the higher the exposure time, the more nanocrystals are formed, leading to a complete degradation of the Cu NWs core. Remarkably, using the HAADF detector, it was possible to confirm that the formation of such NCs is driven by a phenomenon occurring at the surface of the Cu NWs. This is reflected by the experimental detection of NCs formation at the surface of a Cu NW after 10 min of low-reactive plasma exposure as shown in the HAADF micrograph in Fig. 2a.

It is worth emphasising that although the plasma degradation of metallic thin films and nanomaterials have been already reported under high-reactive plasma exposure^{30,37}, the results herein reported and the detailed characterisation presented clearly indicate

Table 1. Crystallographic indexing data for the low-reactive plasma degraded Cu NW (exposure time 25 min).

Experimental data			Crystallographic database values		
Peak Index	d [Å]	Error	Cu ³⁵	CuO ³⁴	Cu ₂ O ³⁶
			d [Å] and reflection planes		
R1	2.43	0.12	–	–	2.464 (1 1 1) ^a
R2	2.05	0.10	2.087 (1 1 1) ^a	–	2.134 (0 0 2)
R3	1.76	0.09	1.808 (0 0 2) ^a	1.797 (1 1 2)	1.743 (1 1 2)
R4	1.48	0.07	–	1.515 (1 1–3)	1.509 (0 2 2) ^a
R5	1.25	0.06	–	1.261 (2 2–2) ^a	1.232 (2 2 2)
R6	1.07	0.05	1.090 (1 1 3) ^a	1.079 (1 3 1)	1.067 (0 0 4)
R7	0.89	0.04	0.904 (0 0 4)	0.899 (2 2 4)	0.871 (2 2 4) ^a
R8	0.79	0.04	0.808 (0 2 4) ^a	0.798 (4 0 4)	0.793 (2 3 4)

Note: The crystallographic database values marked with ^a are satisfying the indexing criterium adopted in this work.

that severe degradation can occur—in the case of single-crystal Cu NWs—even in low-reactive plasma environments.

The degradation of the single-crystal Cu NWs can be empirically interpreted via the electron-beam-induced contrast mechanisms of the HAADF micrographs^{38–40} obtained during the characterisation before and after low-reactive plasma exposure. When imaged with the HAADF detector and along a specific zone axis, the initial single-crystal structure of the Cu NWs is of a complete uniform bright contrast as can be noted in Fig. 1d. But after 10 min of low-reactive plasma exposure—the micrograph in Fig. 2a—the HAADF contrast is strongly changed when compared with the pristine Cu NW in Fig. 1d: this contrast alteration is due to the presence of the randomly oriented NCs at the surface of the plasma-exposed Cu NW. Due to a combination of the HAADF signals emerging from both NCs and NW, at the surface of the latter, the NCs are of brighter contrast. By this, both shape and size of NCs are revealed.

These superficial NCs were further characterised in Fig. 4 where it was observed that they can form at the surface of the Cu NW and then deposit onto a substrate directly beneath the Cu NW. By using the EDX signal from Cu, the sizes of such NCs were estimated to have a bi-modal distribution which has been already associated with characteristic nucleation and growth mechanisms described in the literature^{12,41}.

The hypothesis of surficial degradation triggered by the low-reactive plasma exposure was investigated in-depth via SAED pattern indexing. The EDX measurements presented in Figs 1e, f, 2a, b as well as the overlapped O and Cu maps in Fig. 3 suggest the presence of O at the NW before and after plasma exposure. As mentioned in the results section, the presence of O before plasma exposure is probably associated with a partial passivation layer at the Cu NW surface as metals (at low temperatures) do not dissolve O atoms in solid solution. Using the Cu and O maps, this passivation layer was estimated to have a thickness of around 14.1 ± 1.3 nm. The presence of O within the NW–NCs system persists after low-reactive plasma exposure, which motivated the use of the Cu, CuO and Cu₂O crystallographic data to index the polycrystalline rings in Fig. 5. Giving the limits of detection, the presence of either CuO or Cu₂O cannot be ruled out by the SAED indexing analysis, but this creates an apparent contradiction with the facts that neither O does not show a significant enrichment around the NCs in the EDX maps of the Fig. 2a, b nor the estimated atomic composition after plasma exposure matches with the CuO or Cu₂O oxide phases, although a trend has been detected towards the elemental composition of the latter.

The formation of Cu-rich oxide NCs after low-reactive plasma exposure can be better understood by analysing the reported

thermodynamic data on the Cu–O system and its phase diagrams^{42–45}. It is established that at the nanoscale^{46,47}, conventional thermodynamics does not necessarily correlate nanomaterials with bulk materials^{48,49} due to the large surface-to-volume ratio and the prevalence of surface tension effects⁵⁰; however, these Cu–O phase diagrams are herein used for shedding light on the discussion of the obtained results.

In the Cu–O phase diagrams reported in the literature, for the regime of very low O partial pressures, the formation of oxide phases such as Cu₂O is already thermodynamic favoured. Naturally, upon a reduction of such O partial pressure after purging and plasma generation, the oxide phases can form in non-stoichiometric conditions (i.e. metal rich) given the favourable thermodynamic conditions^{43,51}. It is worth of emphasising that in the plasma chamber, the pressure before Ar gas purging was measured to be around 0.2 and 0.3 mbar after purge. Although no O was intentionally added into the chamber, it is reasonable to assume some O will be present as impurity in the chamber in low O partial pressure, which allows oxide formation off the ideal stoichiometry. In summary, the exposure to a low-reactive plasma induce the formation of small non-stoichiometric NCs of Cu-rich oxide phases, but a reasonable physical mechanism for explaining this phenomenon is still required.

A first hypothesis to shed light on the degradation mechanism observed to occur in pristine Cu NWs is the possibility of Ar ion bombardment within the plasma chamber. The plasma chamber in our work is not equipped with a device to intentionally accelerate Ar ions in a limited set of directions (i.e. it does not generate an Ar ion beam). Under the conditions herein studied, the literature reports that the kinetic energy of Ar ions within a plasma under a pressure of approximately 0.3 mbar is of around 5 eV⁵²; however, the sputtering yield of Cu by Ar ions in this energy range is close to zero^{53–55}. To confirm this, additional experiments of Ar ion bombardment of pristine Cu NWs were performed in this work and are shown in the Supplementary Information file: the results of these experiments demonstrate that Ar ion bombardment itself is not capable of explaining the observed Cu NWs degradation when exposed to a low-reactive plasma.

The mechanism of Cu NW degradation under low-reactive plasma exposure can be better understood using existing models that were recently studied and reviewed by Ostrikov et al.³⁰ regarding the synthesis of metal oxide NWs under exposure to a high-reactive plasma. It has been reported that when an elemental metallic substrate is subjected to a high-reactive plasma (i.e. O-rich plasma), its surface undergoes localised molten nano-regions which can promote the heterogeneous nucleation and growth of metal oxide NWs upon adsorption of O atoms. These nucleation and growth mechanisms—known as SLS and VSS—were already discussed in the introduction.

In contrast to the SLS, the VSS mechanism is responsible for surface degradation of metals with a high melting point, as here for Cu NWs. This model can be adapted to the results reported in this present work on the exposure of single-crystal Cu NWs to a low-reactive plasma. The diagram pictured in Fig. 6 further elaborates this core idea.

In Fig. 6a, the surface of a Cu NW is represented with roughness (or “hillocks”) at the nanoscale, in contact with Argon atoms, along with a residual content of O atoms, thus setting up a low-reactive plasma. The BFTEM micrograph presented in Fig. 6a shows that such nanoroughness is recurrent feature observed in the Cu NWs investigated in this study.

A hypothetical process to explain the low-reactive plasma induced degradation of Cu NWs is exhibited in the scheme presented in Fig. 6b. The presence of monoatomic O atoms within the plasma suggests that a recombination reaction between two O atoms at a hillock site on the Cu NW's surface is possible and likely to occur. Such O recombination reaction is highly

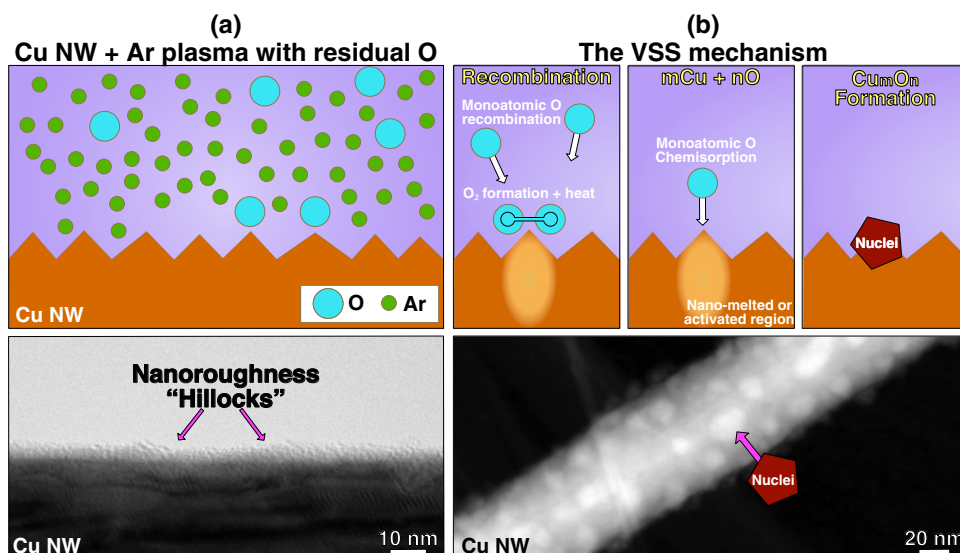


Fig. 6 Proposed sequence for the observed Cu NWs degradation in a low-reactive plasma. An adaptation of the VSS mechanism as a hypothesis to explain the surface-driven degradation of single-crystal Cu NWs. The scheme in **a** shows an initial stage where the plasma is generated and co-exist with the Cu NW; the BFTEM micrograph shows that the Cu NWs used in this work always present nanoroughness at their surfaces. The schemes in **b** show the subsequent stages of monoatomic O recombination, O adsorption and nuclei formation; the micrograph shows that these nuclei are detected using the HAADF detector.

exothermic³⁰; thus, the energy generated can be absorbed at a hillock site and it is sufficient to raise the temperature in a nanoregion. Due to the rapidly increase in the local temperature, monoatomic O chemisorption can occur, which leads to an incorporation of O in the Cu nano-melted region. It should be noted that nanomaterials have a lower melting point than their counterparts^{56–58} and that low-energy Ar ion collisions (on average ≈ 5 eV⁵² for the plasma conditions in this thesis) are able to promote Cu surface diffusion⁵⁹. Both characteristics may facilitate the proposed degradation process. Upon O adsorption, non-stoichiometric Cu oxide nuclei are allowed to form upon cooling. These are the nuclei which are observed as NCs in the HAADF micrographs at the surface of the Cu NWs after plasma exposure. Because of their short-term melting and phase transformation, the compatibility of the nuclei with the NW is greatly reduced, so that they can fall off and the described process takes place repeatedly on the Cu NW surface.

A major distinction between the degradation model herein proposed and the metal oxide nucleation and growth model proposed by Ostrikov et al.³⁰ must be made. In the latter, after nuclei formation and given the high O content in the plasma (i.e. more recombination reactions implying in a higher temperature), a complete metal oxide NW is allowed to grow upon O adsorption. In the former case, given the lower O content, only nuclei are formed, and its crystallised phase is Cu-rich and O-poor.

As experimentally demonstrated in this work, the continuous formation of non-stoichiometric Cu oxide NCs upon exposure of single-crystal Cu NWs to a low-reactive plasma leads to a complete degradation of the NWs core via the destruction of the initial single-crystal structure and characteristic morphology. In contrast to previous works, the present research shows such degradation is able to occur in plasma environments with a low content of O.

A model based on the VSS mechanism has been proposed to explain the observed degradation results. This model assumes that the surface of the initial Cu NWs has nanoroughness (confirmed by electron-microscopy characterisation) which are preferential sites where monoatomic O recombination exothermic reactions are allowed to take place, releasing enough energy to induce local melting of a nanoregion, favouring the formation of such non-stoichiometric Cu oxide NCs upon O consumption via chemisorption.

Although the phenomenon herein observed to occur is referred as degradation of Cu NWs, the results show that this may be an alternative approach for the synthesis of Cu oxide NCs when compared with the existing magnetron-sputtering methods.

Further research is needed to understand the mechanism of non-stoichiometric Cu oxide formation at low pressures as well as more accurate techniques to detect low content of O in the nanometre-sized nuclei. The question whether only metallic Cu NWs are subjected to such observed low-reactive plasma degradation needs further clarification.

METHODS

The experimental methodology used to characterise the degradation effects of low-reactive plasma exposure on single-crystal Cu NWs will be detailed and described in this section.

Sample preparation

Single-crystal Cu NWs in a form of powder was received from Sigma Aldrich. The total mass of Cu NWs was 250 mg and the batch number is MKCL4542. The preparation of a liquid solution was necessary to disperse the NWs. The solution used in this work was made with 8 mg of Cu NWs for 6.8 g of isopropanol. Ultrasonic mixing was used for 30 min before the TEM sample preparation in order to unclutter the Cu NWs in solution. This type of sample preparation for nanomaterials has been described elsewhere^{60,61}.

After ultrasonic mixing, the Cu NWs in solution were pipetted directly onto metallic substrates and left to dry in air. These metallic substrates consisted of 3 mm electro-polished TEM disks. For the experiments reported in this work, different metallic substrates were used, and the results reported here were reproduced using three different substrates (Sn, Al and steel AISI347).

Low-reactive plasma exposure experiments

Plasma exposure was carried out using the plasma cleaning device model FEMTO with a 2.8 L chamber from Diener. The generator was operating at 60% of maximum power which corresponds to 100 W. The frequency of the generator was 40 kHz. The chamber was pumped (pre-purge) to a pressure of 0.2 mbar. At this condition, as a matter of comparison, a quick calculation considering the air as an ideal gas and 1 L of volume (for simplification) shows that at this pressure level, the O₂ concentration is around 414 ppm. Then Ar gas was purged until the pressure stabilised at 0.3 mbar. The used Ar gas was 99.999% pure; therefore, the generated

plasma is herein defined as low-reactive plasma, i.e., a low-content of reactive species may be present, but not intentionally added, due to the vacuum conditions. It is worth emphasising that a pressure level of 0.3 mbar corresponds to the category of medium vacuum, often referred in the literature as not high enough to mitigate the influence of active species such as O^{62} . Therefore, given the residual concentration of monoatomic active species such as O, the term “low-reactive plasma” has been adopted throughout this work. For the experiments reported in this work, plasma exposure was carried out in function of two time lengths: 10 and 25 min.

Electron-microscopy characterisation

For these experiments, a ThermoFisher Scientific™ Talos F200X G2 electron microscope was used. The TEM operated a field-emission gun at 200 kV and it is equipped with Super-X EDX detectors. Before plasma exposure, a TEM pre-characterisation was carried out in the pristine Cu NWs onto metallic 3 mm disks. The edges of the 3 mm disks were used as landmarks to pinpoint specific Cu NWs. After plasma exposure, some Cu NWs were not found in their landmarked areas, most likely because they were washed away during plasma exposure. The pre and post plasma exposure TEM characterisation—under identical conditions—consisted of BFTEM, HAADF and STEM-EDX mapping. SAED patterns using a 660 mm camera length were also recorded to monitor the crystallinity of the NWs. The EDX maps presented in this work were processed in the ThermoFisher Velox software (version 2.9) and represent the net intensities of Cu and O. Elemental quantification was carried out within Velox using the Schreiber-Wims ionisation cross-section model and a multi-polynomial (parabolic) fit function for the EDX spectra. The radius of each quantified NW was measured a priori and this value was used for absorption correction purposes along with a density of 9.0 g cm^{-3} . As the standardless error for elemental composition is around 20% of the value (from the manufacturer⁶³), a set of three different areas were measured for all the quantified NWs reported in this work in order to confirm the estimated compositions within a standard deviation $\leq 5\%$.

DATA AVAILABILITY

The raw and processed data required to reproduce these findings are available to download via the link <https://doi.org/10.17632/ydgcmm2933y.3> permanently stored at the Mendeley Data repository. Correspondence and requests for Cu NWs samples either before or after low-reactive plasma exposure should be addressed to the corresponding author by e-mail: diego.sr.coradini@unileoben.ac.at (D.S.R.C.).

Received: 8 June 2020; Accepted: 11 October 2020;

Published online: 05 November 2020

REFERENCES

- Wang, X. et al. Surface emission characteristics of ZnO nanoparticles. *Chem. Phys. Lett.* **423**, 361–365 (2006).
- Chen, Y. et al. Phase engineering of nanomaterials. *Nat. Rev. Chem.* **4**, 243–356 (2020).
- Hsu, C. L., Tsai, J. Y. & Hsueh, T. J. Novel field emission structure of CuO/Cu₂O composite nanowires based on copper through silicon via technology. *RSC Adv.* **5**, 33762–33766 (2015).
- Flegler, A., Wintzheimer, S., Schneider, M., Gellermann, C. & Mandel, K. In *Handbook of Nanomaterials for Industrial Applications*. (ed. Hussain, C. M.) 137–150 (Elsevier, 2018).
- Shankar, S. & Rhim, J. W. Facile approach for large-scale production of metal and metal oxide nanoparticles and preparation of antibacterial cotton pads. *Carbohydr. Polym.* **163**, 137–145 (2017).
- Mtibe, A., Mokhothu, T. H., John, M. J., Mokhena, T. C. & Mochane, M. J. In *Handbook of Nanomaterials for Industrial Applications*. (ed. Hussain, C. M.) 151–171 (Elsevier, 2018).
- Gibson, B. C. et al. The interaction of atomic oxygen with thin copper films. *J. Chem. Phys.* **96**, 2318–2323 (1992).
- Chau, R., Datta, S. & Majumdar, A. Opportunities and challenges of III-V nanoelectronics for future high-speed, low-power logic applications. In *IEEE Compound Semiconductor Integrated Circuit Symposium 4* (IEEE, 2005).
- Kennedy, J. K. & Friesen, C. The effect of oxygen adsorption on Cu(111) thin film growth stresses. *J. Appl. Phys.* **101**, 054904 (2007).
- Cui, Q., Gao, F., Mukherjee, S. & Gu, Z. Joining and interconnect formation of nanowires and carbon nanotubes for nanoelectronics and nanosystems. *Small* **5**, 1246–1257 (2009).
- Yao, D., Zhang, G. & Li, B. A universal expression of band gap for silicon nanowires of different cross-section geometries. *Nano Lett.* **8**, 4557–4561 (2008).
- Koten, M. A., Voeller, S. A., Patterson, M. M. & Shield, J. E. In situ measurements of plasma properties during gas-condensation of Cu nanoparticles. *J. Appl. Phys.* **119**, 114306 (2016).
- Sutter, P. How silicon leaves the scene. *Nat. Mater.* **8**, 171–172 (2009).
- Kumar, S. in *High-Speed and Lower Power Technologies: Electronics and Photonics* (CRC Press, Boca Raton, 2018).
- Chen, R., Li, Y.-C., Cai, J.-M., Cao, K. & Lee, H.-B.-R. Atomic level deposition to extend Moore's law and beyond. *Int. J. Extreme Manuf.* **2**, 22002 (2020).
- Hanif, I. et al. Ion-beam-induced bending of semiconductor nanowires. *Nanotechnology* **29**, 335701 (2018).
- Gomes, D. R., Turkin, A. A., Vainchtein, D. I. & De Hosson, J. T. M. On the fabrication of micro-and nano-sized objects: the role of interstitial clusters. *J. Mater. Sci.* **53**, 7822–7833 (2018).
- Ovid, Ko, I. A., Valiev, R. Z. & Zhu, Y. T. Review on superior strength and enhanced ductility of metallic nanomaterials. *Prog. Mater. Sci.* **94**, 462–540 (2018).
- Chir, D. & Yeo, R. Plasma process considerations for copper wire bonding. In *35th IEEE/CPMT International Electronics Manufacturing Technology Conference (IEMT)*. 1–3 (Kinta Riverfront Hotel, Ipoh, Perak, Malaysia, 2012).
- Jang, J., Chung, S., Kang, H. & Subramanian, V. P-type CuO and Cu₂O transistors derived from a sol-gel copper (II) acetate monohydrate precursor. *Thin Solid Films* **600**, 157–161 (2016).
- Rai, B. P. Cu₂O solar cells: a review. *Sol. Cells* **25**, 265–272 (1988).
- Li, J., Mayer, J. W. & Colgan, E. G. Oxidation and protection in copper and copper alloy thin films. *J. Appl. Phys.* **70**, 2820–2827 (1991).
- Wang, R. et al. Plasma-induced nanowelding of a copper nanowire network and its application in transparent electrodes and stretchable conductors. *Nano Res.* **9**, 2138–2148 (2016).
- Hsieh, J. H., Fong, L. H., Yi, S. & Metha, G. Plasma cleaning of copper leadframe with Ar and Ar/H₂ gases. *Surf. Coat. Technol.* **112**, 245–249 (1999).
- Kegel, B. & Schmid, H. Low-pressure plasma cleaning of metallic surfaces on industrial scale. *Surf. Coat. Technol.* **112**, 63–66 (1999).
- Wu, F., Levitin, G. & Hess, D. W. Low-temperature etching of Cu by hydrogen-based plasmas. *ACS Appl. Mater. Interfaces* **2**, 2175–2179 (2010).
- Gasparotto, A. et al. Plasma processing of nanomaterials: emerging technologies for sensing and energy applications. *J. Nanosci. Nanotechnol.* **11**, 8206–8213 (2011).
- Lin, L. & Wang, Q. Microplasma: a new generation of technology for functional nanomaterial synthesis. *Plasma Chem. Plasma Process.* **35**, 925–962 (2015).
- Zheng, J. et al. Plasma-assisted approaches in inorganic nanostructure fabrication. *Adv. Mater.* **22**, 1451–1473 (2010).
- Ostrikov, K., Levchenko, I., Cvelbar, U., Sunkara, M. & Mozetic, M. From nucleation to nanowires: a single-step process in reactive plasmas. *Nanoscale* **2**, 2012–2027 (2010).
- Meyyappan, M. A review of plasma enhanced chemical vapour deposition of carbon nanotubes. *J. Phys. D Appl. Phys.* **42**, 213001 (2009).
- Islam, M. S., Sharma, S., Kamins, T. I. & Williams, R. S. A novel interconnection technique for manufacturing nanowire devices. *Appl. Phys. A Mater. Sci. Process.* **80**, 1133–1140 (2005).
- Isabell, T. C., Fischione, P. E., O'Keefe, C., Guruz, M. U. & Dravid, V. P. Plasma cleaning and its applications for electron microscopy. *Microsc. Microanal.* **5**, 126–135 (1999).
- Smura, C. F. et al. High-spin cobalt (II) ions in square planar coordination: structures and magnetism of the oxysulfides Sr₂CoO₂Cu₂S₂ and Ba₂CoO₂Cu₂S₂ and their solid solution. *J. Am. Chem. Soc.* **133**, 2691–2705 (2011).
- Swanson, H. E. & Tatge, E. Standard x-ray diffraction patterns. *J. Res. Natl Bur. Stand.* **46**, 318 (1951).
- Kirfel, A. & Eichhorn, K. Accurate structure analysis with synchrotron radiation. The electron density in Al₂O₃ and Cu₂O. *Acta Cryst. A* **46**, 271–284 (1990).
- Borras, A. et al. Factors that contribute to the growth of AgTiO₂ nanofibers by plasma deposition. *Plasma Process. Polym.* **4**, 515–527 (2007).
- Von Heimendahl, M. *Electron Microscopy of Materials: An Introduction* (Academic Press, 1980).
- Williams, D. B., Carter, C. B. & Veyssièrre, P. *Transmission Electron Microscopy: A Textbook for Materials Science*. Vol. 10 (Springer, 1998).
- Cowley, J. M. STEM imaging with a thin annular detector. *J. Electron Microsc.* **50**, 147–155 (2001).
- Dailey, E. & Drucker, J. “Seedless” vapor-liquid-solid growth of Si and Ge nanowires: the origin of bimodal diameter distributions. *J. Appl. Phys.* **105**, 64317 (2009).
- Hallstedt, B., Risold, D. & Gauckler, L. J. Thermodynamic assessment of the copper-oxygen system. *J. Phase Equilibria* **15**, 483–499 (1994).
- Korzavyi, P. A. & Johansson, B. *Literature Review on the Properties of Cuprous Oxide Cu₂O and the Process of Copper Oxidation* (Swedish Nuclear Fuel and Waste Management Co., 2011).

44. Schramm, L., Behr, G., Löser, W. & Wetzig, K. Thermodynamic reassessment of the Cu–O phase diagram. *J. Phase Equilibria Diffus.* **26**, 605–612 (2005).
45. Shishin, D., Jak, E. & Decterov, S. A. Thermodynamic assessment and database for the Cu–Fe–O–S system. *Calphad* **50**, 144–160 (2015).
46. Park, J. & Lee, J. Phase diagram reassessment of Ag–Au system including size effect. *Calphad* **32**, 135–141 (2008).
47. Liang, L. H., Liu, D. & Jiang, Q. Size-dependent continuous binary solution phase diagram. *Nanotechnology* **14**, 438 (2003).
48. Wang, C. X. & Yang, G. W. Thermodynamics of metastable phase nucleation at the nanoscale. *Mater. Sci. Eng. R* **49**, 157–202 (2005).
49. Yang, C. C. & Mai, Y.-W. Thermodynamics at the nanoscale: a new approach to the investigation of unique physicochemical properties of nanomaterials. *Mater. Sci. Eng. R* **79**, 1–40 (2014).
50. Bedeaux, D. & Kjøstrup, S. Hill's nano-thermodynamics is equivalent with Gibbs' thermodynamics for surfaces of constant curvatures. *Mater. Chem. Lett.* **707**, 40–47 (2018).
51. Saiz, E., Cannon, R. M. & Tomsia, A. P. High-temperature wetting and the work of adhesion in metal/oxide systems. *Annu. Rev. Mater. Res.* **38**, 197–226 (2008).
52. Olthoff, J. K., Vanbrunt, R. J. & Radovanov, S. B. Studies of ion kinetic-energy distributions in the gaseous electronics conference Rf reference cell. *J. Res. Natl Inst. Stand. Technol.* **100**, 383 (1995).
53. Carter, G. & Colligon, J. S. *Ion Bombardment of Solids* (Heinemann Educational Books, 1968).
54. Kress, J. D. et al. Molecular dynamics simulation of Cu and Ar ion sputtering of Cu (111) surfaces. *J. Vac. Sci. Technol.* **17**, 2819–2825 (1999).
55. Colligon, J. & Vishnyakov, V. In Wandelt, K. (ed.), *Surface and Interface Science* Vol. 9, 1–55 (John Wiley & Sons, 2016).
56. Van Teijlingen, A., Davis, S. A. & Hall, S. R. Size-dependent melting point depression of nickel nanoparticles. *Nanoscale Adv.* **2**, 2347–2351 (2020).
57. Kart, H. H., Yildirim, H., Kart, S. O. & Cagin, T. Physical properties of Cu nanoparticles: a molecular dynamics study. *Mater. Chem. Phys.* **147**, 204–212 (2014).
58. Singh, M., Lara, S. & Tlali, S. Effects of size and shape on the specific heat, melting entropy and enthalpy of nanomaterials. *J. Taibah Univ. Sci.* **11**, 922–929 (2017).
59. Rossnagel, S. M. & Robinson, R. S. Surface diffusion activation energy determination using ion beam microtexturing. *J. Vac. Sci. Technol.* **20**, 195–198 (1982).
60. Jiang, K.-L., Zhang, L.-N., Zhang, H.-X. & Fan, S.-S. Method for preparing transmission electron microscope sample. US Pat. Appl. 12/590,664 (2011).
61. Ko, Y. H., Nagaraju, G., Lee, S. H. & Yu, J. S. Facile preparation and optoelectronic properties of CuO nanowires for violet light sensing. *Mater. Lett.* **117**, 217–220 (2014).
62. Raschke, M. B. *Elementary Surface Reactions of Hydrogen and Oxygen on Silicon: An Optical Second Harmonic Investigation* (Herbert Utz Verlag, 1999).
63. Scientific, T. F. *Velox User Manual: Acquisition and Processing* (ThermoFisher Scientific, 2019).

ACKNOWLEDGEMENTS

Funding for this research was provided by the European Research Council (ERC) excellent science grant “TRANSDESIGN” through the Horizon 2020 programme under contract 757961 and by the financial support from the Austrian Research Promotion Agency (FFG) in the project 3DnanoAnalytics (FFG-No 858040). C.G.S. acknowledges the financial assistance of the Brazilian National Research, Development, and Innovation Council (CNPq) through the grant number 308565/2018-5. D.S.R.C. and

M.A.T. would like to thank Mr. Matthias Honner for his support with the Cu NWs solution preparation and to Mr. Luigi Cattini for the support with electron-microscopy.

AUTHOR CONTRIBUTIONS

D.S.R.C. and M.A.T. contributed equally to this manuscript conceptualisation, writing and editing. D.S.R.C. performed all sample preparation. D.S.R.C. and M.A.T. performed all the low-reactive plasma exposure experiments reported in this paper, including the electron-microscopy pre-, post-characterisation and data evaluation under the supervision and assistance of T.M.K. D.S.R.C. and M.A.T. led the manuscript writing together. D.S.R.C. and T.M.K. performed the Ar ion bombardment experiments reported in the Supplementary Information under the supervision of M.A.T. C.G.S., P.J. U. and S.P. contributed with the thermodynamic and metallurgical interpretation of all phenomena reported in the paper. T.M.K., C.G.S., P.J.U. and S.P. contributed with review and editing the manuscript draft. S.P. led the execution of the research, manuscript conceptualisation and secured funding for the research.

COMPETING INTERESTS

The authors declare no competing interests.

ADDITIONAL INFORMATION

Supplementary information is available for this paper at <https://doi.org/10.1038/s41529-020-00137-2>.

Correspondence and requests for materials should be addressed to D.S.R.C. or M.A.T.

Reprints and permission information is available at <http://www.nature.com/reprints>

Publisher's note Springer Nature remains neutral with regard to jurisdictional claims in published maps and institutional affiliations.



Open Access This article is licensed under a Creative Commons Attribution 4.0 International License, which permits use, sharing, adaptation, distribution and reproduction in any medium or format, as long as you give appropriate credit to the original author(s) and the source, provide a link to the Creative Commons license, and indicate if changes were made. The images or other third party material in this article are included in the article's Creative Commons license, unless indicated otherwise in a credit line to the material. If material is not included in the article's Creative Commons license and your intended use is not permitted by statutory regulation or exceeds the permitted use, you will need to obtain permission directly from the copyright holder. To view a copy of this license, visit <http://creativecommons.org/licenses/by/4.0/>.

© The Author(s) 2020